Eur. Phys. J. D **31**, 459–467 (2004)
DOI: 10.1140/epjd/e2004-00148-5

THE EUROPEAN PHYSICAL JOURNAL D

Memory effects in speed-changing collisions and their consequences for spectral line shape

II. From the collision to the Doppler regime

L. Bonamy, H. Tran Thi Ngoc, P. Joubert[a], and D. Robert

Laboratoire de Physique Moléculaire, UMR CNRS 6624, Faculté des Sciences, La Bouloie, Université de Franche-Comté, 25030 Besançon Cedex, France

Received 29 April 2004 / Received in final form 18 June 2004
Published online 3 November 2004 –

Abstract. The kinetic model accounting for speed-memory effects on the spectral line shape proposed in I [D. Robert, L. Bonamy, Eur. Phys. J. D **2**, 245 (1998)] is extended for any density range, within the binary collision framework. The additional Doppler contribution requires to consider the 3D velocity-memory function instead of the 1D speed one, with *distinct* treatments for the velocity-orientation and velocity-modulus memory mechanisms. Both the collisional confinement narrowing of the Doppler distribution and the radiator speed-dependence of the collisional broadening and shifting parameters are thus conveniently taken into account. In the high density regime, this model leads to the same results as in I. At lower densities, it generalizes the very well-known hard and soft collision models for the Dicke narrowing of the Doppler distribution, but it also includes the second source of inhomogeneity tied to the speed-dependent collisional parameters and, concomitantly, the speed class exchanges. Numerical applications to H_2-N_2 and H_2-Ar gaseous mixtures are in close agreement with experiments. This allows one to clearly analyze the *specific* role of speed and velocity memory effects on the line profile.

PACS. 34.10.+x General theories and models of atomic and molecular collisions and interactions (including statistical theories, transition state, stochastic and trajectory models, etc.) – 33.70.Jg Line and band widths, shapes, and shifts

Introduction

High-resolution infrared [1] and Raman [2] spectroscopies require refined spectral line shape model to account for all observed features. For instance, for gaseous mixtures of light molecules with heavy perturbers, drastic changes arise in the collision regime [3,4] resulting from the inhomogeneous effects due to the radiator speed-dependence of the collisional line broadening and line shifting parameters. High temperature enhances such spectral line shape changes, so that a specific interest lies in their study for diagnostics in combusting media [5]. Efficient models based on the hard collision approximation [3,6] have been proposed to fit accurately such inhomogeneous profiles. In these models, the crucial parameter is the ν^{SC} frequency of speed-changing collisions which governs the speed class exchanges. This parameter has been found to be typically one order of magnitude lower than the velocity changing collision frequency ν^{VC} for H_2 in heavy perturbers mixtures [3,4]. This was recently confirmed by molecular dynamics calculations [7]. In order to understand the physical mechanism underlying such a drastic change from the velocity-changing to the speed-changing collision frequency, a kinetic model based on a realistic speed memory function characterized by a unique parameter γ ($0 \leq \gamma \leq 1$) has been proposed in reference [8] (labeled I in the following). It has been demonstrated in I that this kinetic model well accounts for the observed speed inhomogeneous spectral effects in the collision regime (i.e. in the absence of confinement narrowing [9]), i.e. a non linear dependence of the line broadening and the line shifting parameters on perturber concentration, as well as a non Lorentzian asymmetric profile. It allows one to calculate the speed-dependent spectral line shapes at high density from the hard (H) collision approximation [10] (i.e. when each collision thermalizes the radiator speed) up to the opposite soft (S) collision one [11] (i.e. when a significant speed change requires a large number of collisions).

The aim of the present work is to generalize this kinetic model to lower densities, when the Doppler contribution, and the concomitant collisional confinement narrowing [9], can be no longer neglected. Such an intermediate density range between the pure Doppler and the collision regime is relevant for many applications, not only in

[a] e-mail: pierre.joubert@univ-fcomte.fr

combustion but also in atmospheric sciences where the existing models are frequently not accurate enough [12]. The main objective is thus the rigorous study of *both* the collisional confinement narrowing of the Doppler distribution and the inhomogeneous effects due to the radiator speed-dependence of the collisional half width $\gamma_{coll}(v)$ and shift $\delta_{coll}(v)$ on the line shape, within the framework of the impact kinetic equation [10]. As recently evidenced from molecular dynamics simulations [13,14], this requires to introduce *distinct* treatments for the velocity-orientation and velocity-modulus memory mechanisms.

Recent works have been devoted to the speed-dependent line shape problem with Dicke narrowing [15–17]. Starting from a general formalism for solving the transport/relaxation equation [15], May and coworkers have performed numerical calculations within the frame of the rigid sphere approximation for the velocity-changing collision operator by choosing a quadratic speed dependence for the collisional broadening and shifting parameters [16]. The role of the perturber mass, the density, and the ratio of the optical to kinetic cross-section on the resulting line shapes was carefully considered. The main characteristic of this approach is the care to develop a formalism free of phenomenological parameters. Results obtained in the hydrodynamic limit (i.e. when the Doppler shift may be neglected) by Ciurylo et al. [14], have shown the pertinence of such an approach, through a comparison with molecular dynamic simulation data [7]. In an other approach including new phenomenological parameters [17], the Rautian-Sobelman [10] and Keilson-Storer (KS) [18] models were used to describe velocity-changing collisions. Furthermore, the kinetic equation with the KS model [18] has been solved by Shapiro [19] in order to analyze the linewidth behavior vs. the radiator velocity-memory persistence. In these studies [14–18], no distinction between changes in the magnitude and changes in the direction of the velocity was done.

The aim of this paper is precisely to study the role of these two velocity-memory characteristics, in close connection with experimental data for physical situations where the speed inhomogeneous spectral signatures are so large that they can be identified without any ambiguity. Starting from the impact kinetic equation, including the Doppler contribution with a convenient bi-parametric 3D radiator velocity-memory function, the expression for the line shape is established in Section 1. Section 2 is devoted to a numerical study of the velocity and speed memory effects on the spectral distribution with applications to the H_2-N_2 and H_2-Ar systems. Concluding remarks and discussion are given in Section 3.

1 3D kinetic equation and resulting line shape

The velocity-changing collisions (VC) and dephasing collisions (D) may be a priori considered as statistically independent or not, so that these two physical situations will be examined successively.

1.1 Statistical independence of VC and D collisions

If VC and D collisions are assumed to be statistically independent, the kinetic impact equation for the radiating dipole characterized by the velocity $\vec{v}$ at time t is [11]

$$\frac{\partial}{\partial t} d(\vec{v},t) \equiv \dot{d}(\vec{v},t) = - \nu^{VC} \left[d(\vec{v},t) - \int d\vec{v}\,' f^{KS}_{\gamma_{\vec{v}}}(\vec{v}\,',\vec{v}) d(\vec{v}\,',t) \right] - \left[i\vec{k}\cdot\vec{v} + \gamma_{coll}(v) + i\delta_{coll}(v) \right] d(\vec{v},t), \quad (1)$$

where $\vec{k}$ is the radiator wave-vector, ν^{VC} the velocity-changing collision frequency (assumed [10] to be $\vec{v}$-independent), and $f(\vec{v}\,',\vec{v})$ the radiator *velocity*-memory function for the collisionally induced $\vec{v}\,' \to \vec{v}$ transition.

In order to solve equation (1), we must define pertinent eigenfunctions of the 3D integral operator in this kinetic equation. With this aim, the orientational dependence of the velocity-orientation memory function (through the scalar product $\vec{v}\cdot\vec{v}\,' = (\vec{v}^{\,o}\cdot\vec{v}\,'^{o})\, vv'$) may be explicited [19] through the expansion of the memory function in the Legendre polynomials basis $\{P_\ell(\vec{v}\,'^{o},\vec{v}^{\,o})\}$

$$f(\vec{v}\,',\vec{v}) = \frac{1}{2\pi} \sum_{\ell=0}^{\infty} \frac{1}{2}(2\ell+1) f_\ell(v',v) P_\ell(\vec{v}\,'^{o},\vec{v}^{\,o}). \quad (2)$$

If the KS model [18] is chosen to describe this 3D velocity-memory function, a *unique* parameter $\gamma_{\vec{v}}$ ($0 \le \gamma_{\vec{v}} \le 1$) thus governs *both* the speed- and the velocity-orientation memory. Such an assumption is not realistic for most of molecular systems as recently shown from molecular dynamics simulations [13,14]. A convenient bi-parametric memory model has been recently introduced [13] in the following form

$$f_{\gamma_m,\gamma_o}(\vec{v}\,',\vec{v}) = f_{\gamma_m}(v',v)\; f_{\gamma_o}(\vec{v}\,'^{o},\vec{v}^{\,o}), \quad (3)$$

with

$$f_{\gamma_m}(x',x) = \overline{W}_B(x) \sum_{n=0}^{\infty} \gamma_m^{2n} \overline{L}_n^{1/2}(x) \overline{L}_n^{1/2}(x'),$$

$$f_{\gamma_o}(\vec{v}\,'^{o},\vec{v}^{\,o}) = \frac{1}{2\pi} \sum_{\ell=0}^{\infty} \frac{1}{2}(2\ell+1) \gamma_o^\ell P_\ell(\vec{v}\,'^{o},\vec{v}^{\,o}), \quad (4)$$

where $x = mv^2/2kT$. In equation (4), $\overline{W}_B(x)$ means the Boltzmann average for the speed (cf. Eq. (4) of Ref. [8]), $\overline{L}_n^{1/2}(x)$ are the normalized Laguerre Polynomials defined in I, and γ_m, γ_o are respectively the characteristic parameters for modulus- and orientation-velocity memory of the radiator ($0 \le \gamma_m \le 1,\ 0 \le \gamma_o \le 1$). The above memory model (Eqs. (3) and (4)) for v ($\equiv |\vec{v}|$) and $\vec{v}^{\,o}$ ($|\vec{v}^{\,o}| = 1$) has been deduced from pertinent averages [13] over orientation and modulus of the radiator velocity within the frame of the KS model [18]. The corresponding expression for the ℓ-component of this speed memory function is

$$f_\ell(x',x) = \overline{W}_B(x) \gamma_o^\ell \sum_{n=0}^{\infty} \gamma_m^{2n} \overline{L}_n^{1/2}(x) \overline{L}_n^{1/2}(x'). \quad (5)$$

The product of the spherical harmonics $Y_{\ell,m}(\vec{v}^{\,o})$ by the functions $\overline{L}_n^{1/2}(x)$ are eigenfunctions of the 3D integral operator in the kinetic equation (1) for the bi-parametric memory model (Eqs. (4) and (5)) [20,21]. So, the radiation dipole may be expanded over these $Y_{\ell,m}(\vec{v}_i^{\,o})\, L_n^{1/2}(x)$ normalized eigenfunctions

$$d(\vec{v},t) \equiv d(x,\vec{v}^{\,o},t) = \overline{W_B}(x) \sum_{n,\ell,m} a_{n,\ell,m}(t) Y_{\ell,m}(\vec{v}^{\,o}) \overline{L}_n^{1/2}(x), \quad (6)$$

with

$$a_{n,\ell,m}(t) = \int_0^\infty dx\; \overline{L}_n^{1/2}(x)\, d_{\ell,m}(x,t), \quad (7)$$

and

$$d_{\ell,m}(x,t) = \int d\vec{v}^{\,o} d(\vec{v},t) Y^*_{\ell,m}(\vec{v}^{\,o}). \quad (8)$$

From the equilibrium initial condition $d(\vec{v}, t=0) = W_B(\vec{v})$, equations (7) and (8) result in

$$a_{n,\ell,m}(t=0) = \delta_{n,o}\delta_{\ell,o}\delta_{m,o}. \quad (9)$$

Taking the Laplace transform of $d(t) = \int d\vec{v}\; d(\vec{v},t)$,

$$d(\tilde{\omega}) = \int_0^\infty dt\; e^{i\tilde{\omega}t} d(t), \quad (10)$$

the line profile $I(\tilde{\omega})$ is defined by (cf. Eq. (9) of Ref. [8])

$$I(\tilde{\omega}) = \pi^{-1}\, \mathrm{Re}\, \{a_{o,o,o}(\tilde{\omega})\}. \quad (11)$$

Notice that in equations (10) and (11), $\tilde{\omega}$ means the detuned frequency from the rovibrational frequency ω_o of the optically active molecule, $\tilde{\omega} = \omega - \omega_o$.

Multiplying the kinetic equation (1) by $Y^*_{\ell,m}(\vec{v}^{\,o})$ and integrating over all the orientation $\vec{v}^{\,o}$ leads to (cf. Eqs. (6–8)),

$$\dot{d}_{\ell,m}(x,t) + i\Delta\omega_D\, x^{1/2} \left[C_{\ell+1,m} d_{\ell+1,m}(x,t) + C_{\ell,m} d_{\ell-1,m}(x,t)\right] + \left[\nu^{VC} + \gamma_{coll}(x) + i\delta_{coll}(x)\right] d_{\ell,m}(x,t) = \nu^{VC} \int dx' f_\ell(x',x) d_{\ell,m}(x',t), \quad (12)$$

where $f_\ell(x',x)$ is defined by equations (3) and (4) for the ℓ-component, $C_{\ell,m} = ((\ell^2-m^2)/(2\ell-1)(2\ell+1))^{1/2}$, $\Delta\omega_D = (\omega_o/c)\sqrt{2kT/m}$ is the Doppler frequency distribution and c the light velocity. By using the orthogonality of the $Y_{\ell,m}(\vec{v}^{\,o})\overline{L}_n^{1/2}(x)$ eigenfunctions, it is easy to deduce the resulting equation for the $a_{n,\ell,m}(t)$ components of the radiating dipole (cf. Eq. (6)),

$$\dot{a}_{n,\ell,m}(t) + i\Delta\omega_D \left[C_{\ell+1,m} \sum_{n'=0}^\infty I_{nn'} a_{n',\ell+1,m}(t) + C_{\ell,m} \sum_{n'=0}^\infty I_{nn'} a_{n',\ell-1,m}(t)\right] + \nu^{VC}\left(1-\gamma_m^{2n}\,\gamma_o^\ell\right)\, a_{n,\ell,m}(t) + \sum_{n'=0}^\infty \Gamma_{nn'} a_{n',\ell,m}(t) = 0, \quad (13)$$

where

$$I_{nn'} = \int_0^\infty dx \overline{W}_B(x) \overline{L}_n^{1/2}(x) x^{1/2} \overline{L}_{n'}^{1/2}(x), \quad (14)$$

and

$$\Gamma_{nn'} = \int_0^\infty dx\, \overline{W_B}(x)\; \overline{L}_n^{1/2}(x) \times \left[\gamma_{coll}(x) + i\delta_{coll}(x)\right]\, \overline{L}_{n'}^{1/2}(x). \quad (15)$$

For sufficiently high densities, such that the Doppler contribution becomes negligible (the $\vec{k}\cdot\vec{v}$ term in equation (1) can thus be omitted), the $\ell = 0$ component is only to be considered and thus equation (13) reduces to (17) of I (with γ_m substituted to γ). For densities such that the collisional effects can be neglected, equation (13) leads straightforwardly to the Gaussian Doppler profile.

In order to simplify the presentation of the numerical method for the resolution of equation (13), this equation is rewritten in a condensed form as

$$\dot{a}_{n\ell}(t) + \sum_{\substack{\ell'=\ell,\\ \ell\pm1}} \sum_{n'=0}^\infty W_{nn'}^{(\ell,\ell')}\, a_{n'\ell'}(t) = 0, \quad (16)$$

with

$$\begin{aligned} W_{nn}^{(\ell,\ell)} &= \left[\nu^{VC}\left(1-\gamma_m^{2n}\gamma_o^\ell\right)\delta_{nn'} + \Gamma_{nn'}\right], \\ W_{nn'}^{(\ell,\ell+1)} &= i\Delta\omega_D C_{\ell+1} I_{nn'}, \\ W_{nn'}^{(\ell,\ell-1)} &= i\Delta\omega_D C_\ell I_{nn'}. \end{aligned} \quad (17)$$

The m index has been omitted in equations (16) and (17), since the W matrix is diagonal in m and that only the $m=0$ component of the $\{a_{n'\ell'm'}\}$ coefficients is implied in the calculation of the spectral line profile $I(\tilde{\omega})$ (cf. Eq. (11)). It is worthy to note that $W_{nn'}^{(\ell,\ell')}$ is an element of a tridiagonal matrix of ($W^{(\ell,\ell+1)}, W^{(\ell,\ell)}$ and $W^{(\ell,\ell-1)}$) matrices, satisfying the symmetry property

$$W_{n'n}^{(\ell+1,\ell)} = W_{nn'}^{(\ell,\ell+1)}. \quad (18)$$

The Laplace transform (Eq. (10)) of equation (16) is

$$(-i\tilde{\omega} + W)\mathbf{a}(\tilde{\omega}) = \mathbf{1}_{00}, \quad (19)$$

where the initial condition $\mathbf{a}(t=0) = \mathbf{1}_{00}$ has been used (cf. Eq. (9)). If S means the matrix diagonalizing W, the resulting line profile is

$$I(\tilde{\omega}) = \pi^{-1}\ \mathrm{Re}\{a_{00}(\tilde{\omega})\} = \pi^{-1}\left\{\sum_k \sum_q \frac{S_{00,kq}(S^{-1})_{00,kq}}{i\tilde{\omega} + D_{kq}}\right\}, \qquad (20)$$

where the diagonal D matrix is given by $D = S^{-1}\ WS$.

Due to the tridiagonal structure of the W matrix, an alternative method may be used which avoids the diagonalization procedure. Indeed, from equation (19), it results that

$$a_{00}(\tilde{\omega}) = \mathrm{Re}(-i\tilde{\omega} + W)^{-1}_{00,00} \equiv \mathrm{Re}\ \tilde{W}^{-1}_{00,00}, \qquad (21)$$

where $\tilde{W}(\tilde{\omega}) = W - i\tilde{\omega}$. The determination of the diagonal matrix element $n = 0$, $\ell = 0$ of the inverse matrix $\tilde{W}^{-1}$ only requires that of the column of matrices $(\ell, 0)$ in $\tilde{W}^{-1}$. These matrices $\tilde{W}^{-1(\ell,0)}$ $(\ell = 0, ..., \ell_{max})$ can be directly expressed from the known $\tilde{W}^{(0,0)-1}$ and $\tilde{W}^{(0,1)}$ matrices by using a generalization of the forward and backward substitution methods [22] for tridiagonal matrix to tridiagonal matrix of matrices (Appendix A).

In practice the ℓ_{max} value, corresponding to the truncation procedure (Eq. (A.5)), must be chosen to insure the numerical convergence for $a_{00}(t)$ (Eqs. (13) and (16)) whatever the method used (diagonalization or substitution, cf. supra). Furthermore, in each block matrix $W^{(\ell,\ell')}$, the n maximum value must also be fixed from pertinent tests. This second truncature was discussed in I for the 1D case. These technical points concerning the choice of ℓ_{max} and n_{max}, in connection with the convergence of the solution of the kinetic equation, will be carefully analyzed in the next section through the study of the H_2-N_2 and H_2-Ar systems.

1.2 Statistical dependence of VC and D collisions

In the case where the velocity-changing (VC) and dephasing (D) collisions are considered as statistically dependent [10], the following kinetic equation must be substituted to equation (1)

$$\dot{d}(\vec{v},t) = -\nu^{VC}[d(\vec{v},t) - \int d\vec{v}\,' f_{\gamma_m,\gamma_o}(\vec{v}\,',\vec{v})d(\vec{v}\,',t)] - [i\vec{k}\cdot\vec{v} + \gamma_{coll}(v) + i\delta_{coll}(v)]\int d\vec{v}\,' f_{\gamma_m,\gamma_o}(\vec{v}\,',\vec{v})d(\vec{v}\,',t), \qquad (22)$$

where $f_{\gamma_m,\gamma_o}(\vec{v}\,',\vec{v})$ is given by equations (3) and (4). By using the same expansion for $d(\vec{v},t)$ as in Section 2.1 (cf. Eq. (6)), the resulting kinetic equation for the corresponding $a_{n,\ell,m}(t)$ expansion coefficients is formally identical to equation (16) with the following modification

$$W^{(\ell,\ell)}_{nn'} = \left[\nu^{VC}(1 - \gamma_m^{2n}\gamma_o^{\ell})\delta_{nn'} + \gamma_m^{2n'}\gamma_o^{\ell}\Gamma_{nn'}\right], \qquad (23)$$

where $I_{nn'}$ and $\Gamma_{nn'}$ are defined through equations (14) and (15) respectively. The only change with respect to equation (13) induced by the statistical dependence of VC and D collision is thus the presence of the $\gamma_m^{2n'}\gamma_o^{\ell}$ term in the last number of equation (23) (cf. Eq. (17)). Consequently, all the numerical procedure proposed in Section 2.1 to get the spectral line shape (cf. Eqs. (11) and (20)) remains pertinent and will be used in the following section to analyze the role of this VC and D statistical dependence.

2 Numerical study of velocity memory effects on H_2-N_2 and H_2-Ar line shapes

This study is divided in two main parts. The first one concerns a comparison between experimental results and the present bi-parametric approach for a physical system H_2-N_2 of practical interest. The second part is devoted to an extensive study of the influence of the two memory parameters on the spectral lineshape characteristics (line broadening and line asymmetry).

2.1 Comparison to H_2-N_2 experimental data

To test the numerical approach described in the previous section, the H_2-N_2 system will be analyzed in detail. This molecular system exhibits strong inhomogeneous effects for high densities due to the lightness of H_2 molecule and its anharmonicity [23]. It is also of particular interest for optical diagnostic in combustion engines [5,24]. Experiments for highly diluted H_2 in N_2 have been performed by high resolution Inverse Raman Spectroscopy at the University of Dijon for various densities lying between 0.2 (Doppler regime) and 11 amagat (collision domain), and three temperatures (296, 795 and 1200 K) [25]. To explain the important role of both velocity memory parameters (γ_m for speed and γ_o for orientation), we show in Figure 1 the comparison between experimental line widths measured in Dijon University and calculated ones using the mono-parametric KS memory function vs. density ρ at 296 K (cf. Sect. 2.1, Eq. (13) and Ref. [26] with γ substituted to γ_m). Similar curves are obtained at 795 K and 1200 K. From previous studies [2–4], the speed memory parameter plays an important role in the collisional regime (typically for densities higher than a few amagat units). In the opposite case corresponding to Dicke and Doppler regimes, the orientation velocity memory parameter is dominant. The curves reported in Figure 1 fully confirm these assumptions. The agreement between experimental and simulated values is consistently satisfactory at high density using the unique memory parameter $\gamma = 0.92$ (solid line), and at low density with $\gamma = 0$ (dotted line) (cf. Fig. 1). As obtained by molecular dynamic simulations [13], the expected parameters for such a H_2-N_2 system are equal to 0.92 for the γ_m speed memory and to 0.41 for the γ_o orientation velocity one. For intermediate densities (Dicke regime), this mono-parametric approach

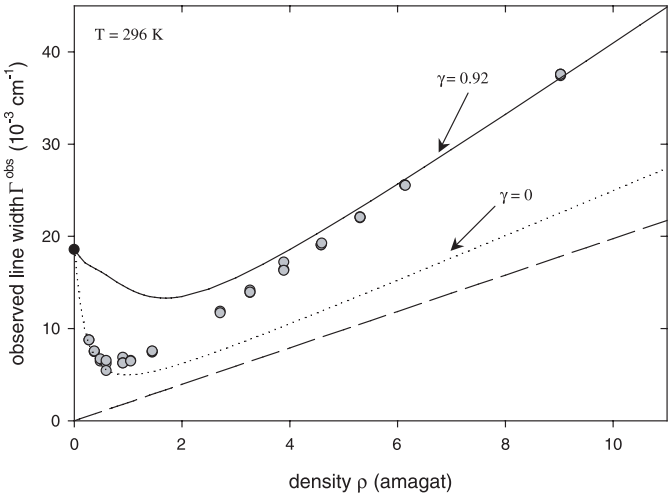

Fig. 1. The observed linewidth Γ^{obs} of the H_2 Q(1) line obtained with 5% of H_2 in 95% of N_2 is plotted vs. density ρ (shaded circles) at 296 K and compared with the line broadening calculated from the monoparametric KS memory function (cf. Eq. (13) with γ substituted to γ_m) for $\gamma = 0.92$ (solid line) and $\gamma = 0$ (dotted line). The collisional line broadening $\gamma_{coll} \times \rho$ (dashed line) is also reported.

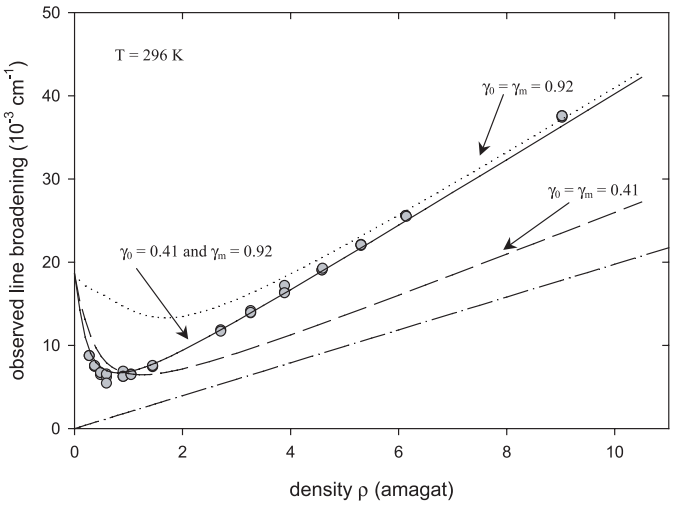

Fig. 2. The observed linewidths Γ^{obs} of the H_2 Q(1) line are compared with the line broadening calculated from the biparametric extended KS memory function (cf. Eq. (13)) for $\gamma_m = 0.92$ and $\gamma_o = 0.41$ (solid line) vs. density ρ at 296 K and 5% of H_2 in 95% of N_2. For comparison, the results obtained with the monoparametric KS memory function (Ref. [26]) are also reported for $\gamma = 0.41$ (dashed line) and $\gamma = 0.92$ (dotted line). The collisional line broadening $\gamma_{coll} \times \rho$ (dotted-dashed line) is also reported.

cannot reproduce accurately the experimental line broadening. It is then clear that two distinct memory parameters are necessary to be able to describe all the lineshapes observed for a very large domain of temperature, concentration and density using a unique profile modelization.

The same comparison for the H_2-N_2 system is presented in Figure 2 vs. density ρ using now the biparametric approach presented in this paper with no statistical correlation between VC and D collisions (cf. Sect. 2.1, Eq. (13)). The agreement between experimental and calculated line widths is very good for all densities studied. It is important to note that no fitting procedure is performed here. The values used for the memory parameters ($\gamma_o = 0.41$ and $\gamma_m = 0.92$) are directly deduced from the molecular dynamic simulations [13]. To improve this agreement, it would be possible to fit the memory parameters from the available experimental data [23,25]. The resulting values would be too close from those obtained from molecular dynamics to justify such a procedure in this case. This result is a further drastic test of the simulation made by molecular dynamics in reference [13]. We can note that a similar agreement is obtained for the two other temperatures ($T = 795$ and 1200 K).

2.2 Influence of the two memory parameters (speed modulus and orientation) on spectral line shapes

We choose to test the accuracy of the bi-parametric approach and specially the influence of both memory parameters (γ_o for orientation and γ_m for modulus) on the line profiles. In this study, we used the H_2-Ar system which exhibits even stronger inhomogeneous effects than for H_2-N_2, due to the presence of a heavier perturber [2,4]. Line widths are reported for different values of γ_o and γ_m memory parameters at two characteristic density regimes in Figure 3 (Dicke: Fig. 3a and collisional ones: Fig. 3b), with the assumption of statistical independence of VC and D collisions (cf. Sect. 1.1). As expected, we have verified the speed memory parameter (γ_m) has nearly no influence at low density. The behaviour is opposite at high density (cf. Fig. 3b), where it is the speed memory which only governs the inhomogeneous broadening. At intermediate density (Fig. 3a) both γ_m and γ_o play a significant role for H_2-Ar. That should be no longer the case for heavy active molecules exhibiting a γ_m value below 0.5. In this case, only orientation memory becomes pertinent as usually known in the Dicke regime [9]. The present biparametric approach confirms the previous H_2-X data analysis [2,4] in terms of velocity memory mechanisms. Notice the strong increase of the inhomogeneous part of the line broadening at 10 amagat (Fig. 3b) when the speed memory parameter (γ_m) is close to its maximum value 1. Let us recall that the inhomogeneous part for H_2-Ar at density higher than few amagat units is of the same order of magnitude as the collisional part, and cannot be neglected. For H_2 in mixtures with heavy perturbers, this inhomogeneous effect must be taken into account for an accurate high pressure thermometry based on Coherent Anti-Stokes Spectroscopy (CARS) [5,24]. A last comment should be made on the collision regime (Fig. 3b). For most molecular systems, (except light optically active molecules with heavy perturbers) from molecular dynamics simulations [7,13], it is expected that $\gamma_m < 0.5$. Consequently, the apparent broadening is thus nearly independent of both γ_m and γ_o. However, notice that for γ_o close to 1, which corresponds to the soft memory process [10,11],

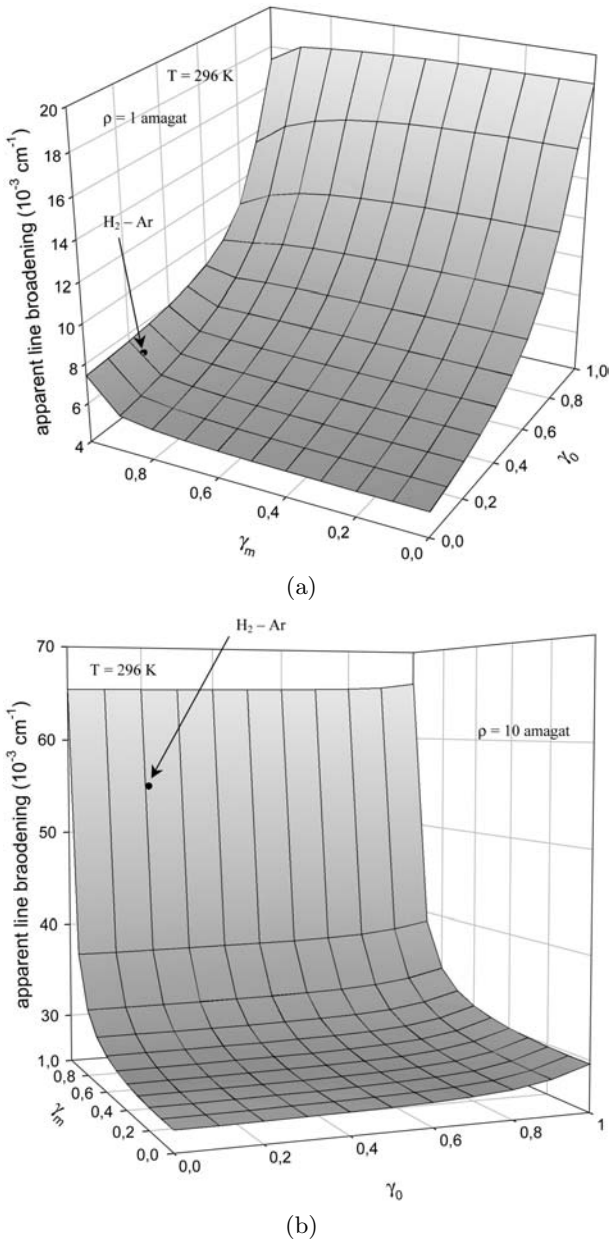

Fig. 3. Calculated line broadening coefficient for H_2 (5%) — Q(1) line perturbed by argon (95%) at 300 K vs. orientation memory parameter (γ_o) and speed memory parameter (γ_m) using the biparametric extended KS memory function (cf. Eqs. (13)). (a) Dicke regime ($d = 1$ amagat) and (b) collisional regime ($d = 10$ amagat). The full circle corresponds to the calculated value by using the values $\gamma_m = 0.96$ and $\gamma_o = 0.21$ resulting from the simulation [13].

the present calculation (Fig. 3b) predicts an orientation velocity memory inhomogeneous broadening.

The second point of interest concerns the correlation effect on spectral lineshapes. As explained in the previous part, the velocity-changing collisions and dephasing collisions may be considered as statistically independent or not. In this part, we propose to discuss the statistical dependence effect on spectral lineshape. As shown in

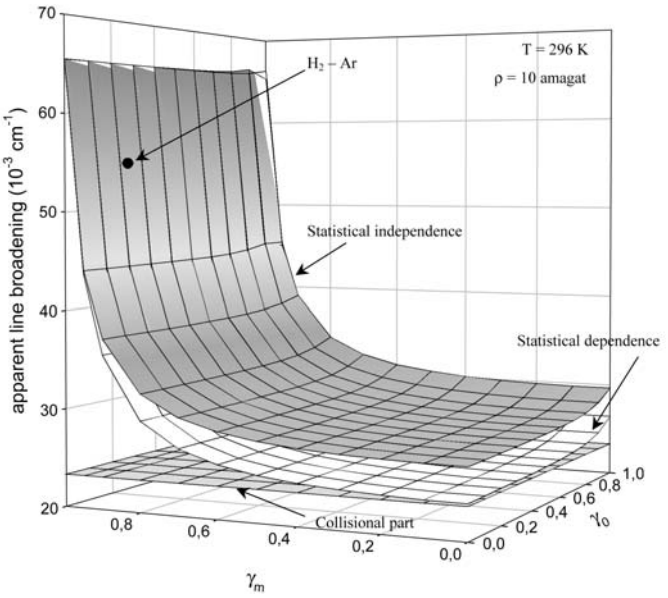

Fig. 4. Calculated line broadening for H_2 (5%) — Q(1) line perturbed by argon (95%) at 300 K and 10 amagat vs. orientation memory parameter (γ_o) and speed memory parameter (γ_m). Comparison between statistical independence of VC and D collisions using the bipamaretric extended KS approach (cf. Eqs. (13) and (14)) and statistical dependence ones (cf. Eq. (23)). The full circle corresponds to the calculated value by using the values $\gamma_m = 0.96$ and $\gamma_o = 0.21$ resulting from the simulation [13].

the previous studies [3,6,27], the statistical dependence between VC and D collisions remains without any significant effect on the observed line width in the collision regime (high density) and when inhomogeneous effects are strong ($\gamma_m \geq 0.8$), i.e. for H_2-X systems where X is an heavy perturber. We have reported in Figure 4 the calculated line widths obtained by correlated and non correlated approaches at high density (10 amagat). It is clear that for high values of speed modulus memory parameter ($\gamma_m \geq 0.8$), no differences between the two calculations can be observed. In this case, the inhomogeneous effect due to the speed dependence of collisional parameters is predominant to the statistical dependence effects. The main differences arise for low values of γ_m corresponding to small inhomogeneous effect on line profiles, regardless of the γ_o value. Indeed, at high density, the speed orientational memory parameter plays no significant role in the speed memory processes. For VC and D correlated collisions, the observed line broadening tends to the collisional one for decreasing values of the γ_m parameter. In the opposite case (non correlated collisions), a difference of 10 to 15% is still observed with the collisional line broadening value [3]. These last results are interesting for systems involving heavy active molecules like H_2O or CO. In this case, inhomogeneous effects are negligible (γ_m lower than 0.5) compared to correlations between VC and D collisions which would have a significant role on the spectral lineshape signature. For intermediate densities, the influence of modulus memory parameter decreases,

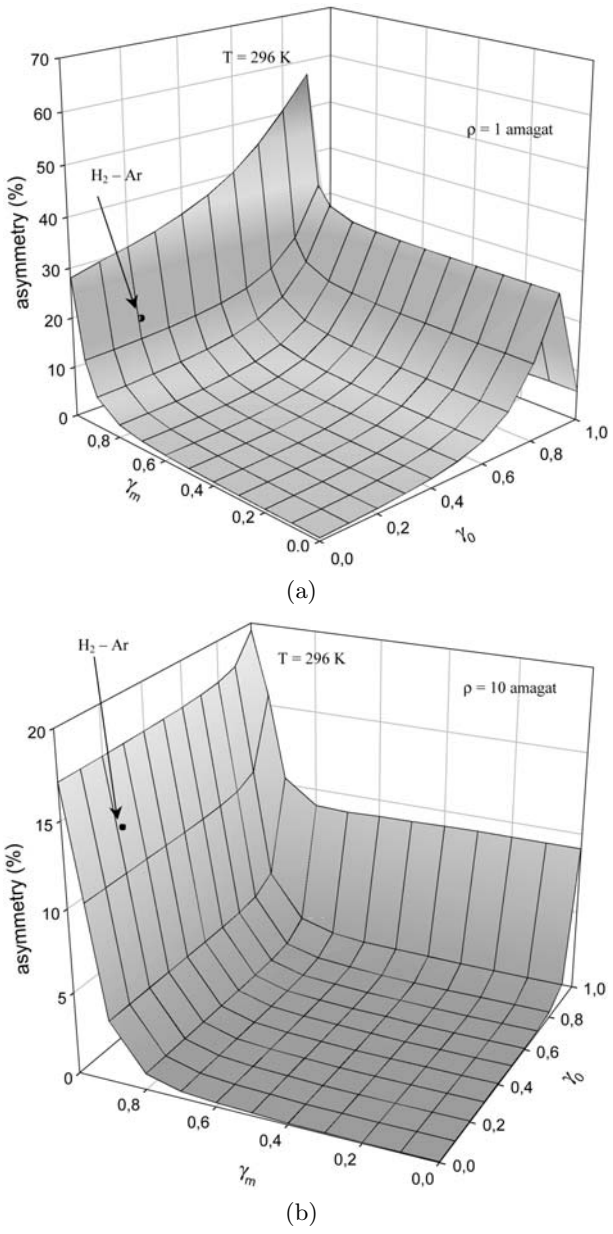

Fig. 5. Calculated asymmetry for H_2 (5%) — Q(1) line perturbed by argon (95%) at 300 K vs. orientation memory parameter (γ_o) and speed memory parameter (γ_m) using the biparametric extended KS memory function (cf. Eqs. (13) and (14)). (a) Dicke regime (d = 1 amagat) and (b) collisional regime (d = 10 amagat). The full circle corresponds to the calculated value by using the values $\gamma_m = 0.96$ and $\gamma_o = 0.21$ resulting from the simulation [13].

calculated line broadenings are nearly identical with the two approaches (correlation and non correlation). At low density regime, the two memory parameters have no significant influence. The line profile is described by the Gaussian Doppler profile, not depending on the correlation of VD and D collisions.

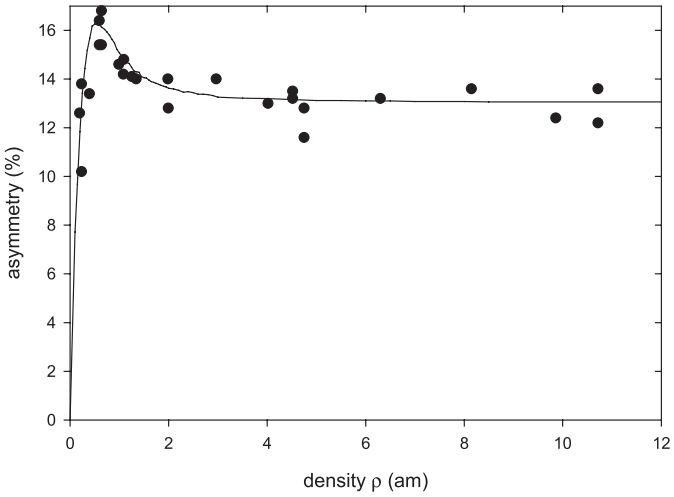

Fig. 6. The experimental asymmetry parameter A of the H_2 Q(1) line obtained with 5% of H_2 and 95% of Ar is plotted vs. density ρ (shaded circles) at 296 K and compared with the asymmetry parameter calculated using the non correlated biparametric extended KS memory function (solid line). The memory parameters $\gamma_m = 0.96$ and $\gamma_o = 0.21$ are deduced from simulation [13].

The last point of interest is the behavior of the line shape asymmetry in each density regime. We defined the asymmetry parameter A as $A = [\nu_{LF} + \nu_{HF} - 2\,\nu_{max}]/\Gamma$ where ν_{HF} and ν_{LF} are the high and low frequencies at half maximum respectively, ν_{max} the frequency at the maximum intensity and Γ the HWHM. The asymmetry, obtained from the calculation of the profiles with the non correlated extended biparametric KS approach is reported in Figure 5. First, it is interesting to note that, at low density (sub-Dicke) regime, the asymmetry coefficient becomes independent of the two velocity memory parameters and is close to 0 for most of (γ_m, γ_o) values except for γ_m and/or γ_o close to 1. The line profile must be symmetric at very low density since it is Gaussian in the Doppler regime. We have tested this specific point through calculations at $d = 0.01$ amagat (not reported here). In the collision regime (i.e. above few amagat units), the asymmetry becomes, as expected, *density-independent*. As for the line broadening (Fig. 3b), the line asymmetry (Fig. 5) only depends on γ_m (except for γ_o close to 1) in this regime. In the Dicke regime, the asymmetry parameter becomes strongly dependent on the velocity orientation parameter. The speed memory has nearly no influence on the value of the asymmetry, except for γ_m values close to 1. For H_2-Ar mixture at 296 K, we show in Figure 6 the comparison between experimental data [2,4] and calculated values of the asymmetry parameter for the γ_m and γ_o data resulting from the simulation [13]. Some instabilities are observed due to the difficulty to extract asymmetry parameter from experimental data. Nevertheless, the agreement remains, as for the broadening, (cf. Fig. 2), still satisfactory.

3 Conclusion

We present in this paper an *extension*, for any density range, of the 1D kinetic model [8] accounting not only for speed-memory effects on the spectral line shape but also for the Doppler contribution. This model is built via two distinct velocity memory parameters (γ_o for orientation and γ_m for modulus). A comparison between experimental data (line broadening and asymmetry) and calculated ones from this new bi-parametric extended KS approach has been performed. It shows a very good agreement for the systems H_2-N_2 and H_2-Ar. These molecular systems are of particular interest for a rigorous tests of this approach since they present strong inhomogeneous effects at high density. To test the model, calculations have been performed for all the validity domain of the two memory parameters (speed γ_m and orientation γ_o lying between 0 and 1). This study allows us to fully analyze all the inhomogeneous effects from the Doppler to the collision regime. This fully confirms all the previous studies [23,25] and introduces further the possibility to discriminate the inhomogeneous contribution in terms of speed memory and velocity orientation ones. As a consequence, this new bi-parametric model of line shape should apply to various molecular systems and at any density range consistent with the binary collision approximation. In the aim of applications for optical diagnostic in combustion media or in atmospheric environments, this approach could be used to increase the accuracy of such optical techniques. In the case of the earth atmosphere, the velocity orientation memory can be dominant. This contrasts with the H_2-X systems at higher density studied here, where this is the velocity modulus memory which plays the dominant role in the line shape. Recent results obtained by a group in Orsay University for H_2O perturbed by N_2 at subatmospheric pressure show typical behaviors not yet explained [28]. A collaboration with this group is now beginning to try to interpret these results through memory effects using the present bi-parametric extended KS model. New approaches to describe the speed dependent laws of collisional parameters (line broadening and line shifting) applied to this model are in progress in the aim to study atmospheric molecular systems, particularly the influence of the correlation on the spectral lineshapes.

The authors greatly acknowledge H. Berger and F. Chaussard, from University of Dijon (France), for providing them experimental spectra.

Appendix A: Forward and backward substitution method for a tridiagonal matrix of matrices

Due to the tridiagonal structure of the $\tilde{W}$ matrix, (cf. Eqs. (15), (17) and (18)) it can be shown by an elimination method that the block $(\ell, 0)$ in the $\tilde{W}^{-1}$ matrix must obey the following recurrence relation

$$\left[\tilde{W}^{-1}\right]^{(\ell,0)} = S^{(\ell)} - T^{(\ell)} \left[\tilde{W}^{-1}\right]^{(\ell+1,0)}, \quad \text{(A.1)}$$

where the couple of matrices $(S^{(\ell)}, T^{(\ell)})$ are also obtained from recurrence relations

$$S^{(\ell)} = [\tilde{W}^{(\ell,\ell-1)} T^{(\ell-1)} - \tilde{W}^{(\ell,\ell)}]^{-1}\, \tilde{W}^{(\ell,\ell-1)} S^{(\ell-1)}, \quad \text{(A.2)}$$

and

$$T^{(\ell)} = [\tilde{W}^{(\ell,\ell-1)} T^{(\ell-1)} - \tilde{W}^{(\ell,\ell)}]^{-1}\, \tilde{W}^{(\ell,\ell+1)}, \quad \text{(A.3)}$$

with the initial conditions

$$S^{(0)} = [\tilde{W}^{(0,0)}]^{-1}, \quad T^{(0)} = [\tilde{W}^{(0,0)}]^{-1}\, \tilde{W}^{(0,1)}. \quad \text{(A.4)}$$

Notice that $[\tilde{W}^{(0,0)}]^{-1}$ means the inverse of the $(0,0)$ block matrix in the known (total) matrix $\tilde{W}$ (cf. Eqs. (17) and (18)), which corresponds to the 1D case of I in the absence of the Doppler contribution in the kinetic equation (1). This matrix being of infinite order (both in ℓ and in n), we first introduce a maximum value ℓ_{max} for ℓ through a truncation procedure defined by

$$\tilde{W}^{(\ell_{max},\ell_{max}+1)} = 0. \quad \text{(A.5)}$$

From this truncation, it follows that

$$\tilde{W}^{(\ell_{max}-1,\ell_{max})} \left[\tilde{W}^{-1}\right]^{(\ell_{max}-1,0)} + \tilde{W}^{(\ell_{max},\ell_{max})} \left[\tilde{W}^{-1}\right]^{(\ell_{max},0)} = 0. \quad \text{(A.6)}$$

Accounting for equation (A.6) in equation(A.1) for $\ell = \ell_{max} - 1$ permits to deduce the $[\tilde{W}^{-1}]^{(\ell_{max}-1)}$ matrix, since it is easy to show, through an identification with equation (A.2) for $\ell = \ell_{max}$, that

$$\left[\tilde{W}^{-1}\right]^{(\ell_{max},0)} = S^{(\ell_{max})}. \quad \text{(A.7)}$$

This forward substitution starting from the initial conditions (A.4), allows one to built all the $S^{(\ell)}$ and $T^{(\ell)}$ matrices for ℓ going from 0 to $\ell_{max} - 1$, plus the $S^{(\ell_{max})}$ one (the $T^{(\ell_{max})}$ being zero due to the truncation (A.5)). A further backward substitution starting from $[\tilde{W}^{-1}]^{(\ell_{max},0)}$ is thus done from the recurrence relation (A.1) to get all the $[\tilde{W}^{-1}]^{(\ell,0)}$ block matrices for ℓ going from ℓ_{max} to 0, as required to numerically solve equations (16) or (22) through equations (20) and (21).

References

1. P. Duggan, P.M. Sinclair, R. Berman, J.R. Drummond, J. Mol. Spectrosc. **186**, 90 (1997)
2. F. Chaussard, X. Michaut, R. Saint-Loup, H. Berger, P. Joubert, B. Lance, J. Bonamy, D. Robert, J. Chem. Phys. **112**, 158 (2000)

3. R.L. Farrow, L.A. Rahn, G.O. Sitz, G.J. Rosasco, Phys. Rev. Lett. **63**, 746 (1989)
4. J.Ph. Berger, R. Saint-Loup, H. Berger, J. Bonamy, D. Robert, Phys. Rev. A **49**, 3396 (1994)
5. J. Hussong, W. Stricker, X. Bruet, P. Joubert, J. Bonamy, D. Robert, X. Michaut, T. Gabard, H. Berger, Appl. Phys. B **70**, 447 (2000)
6. D. Robert, J.M. Thuet, J. Bonamy, S. Temkin, Phys. Rev. A **47**, 771 (1993)
7. P.N.M. Hoang, P. Joubert, D. Robert, Phys. Rev. A **65**, 012507 (2002)
8. D. Robert, L. Bonamy, Eur. J. Phys. D **2**, 245 (1998)
9. R.H. Dicke, Phys. Rev. **89**, 472 (1953)
10. S.G. Rautian, I.I. Sobel'man, Sov. Phys. Uspekhi. **9**, 701 (1967)
11. L. Galatry, Phys. Rev. **122**, 1218 (1961)
12. R. Berman, P.M. Sinclair, A.D. May, J.R. Drummond, J. Mol. Spectrosc. **198**, 283 (1999)
13. P. Joubert, P.N.M. Hoang, L. Bonamy, D. Robert, Phys. Rev. A **66**, 042508 (2002)
14. R. Ciurylo, D. Lisak, J. Szudy, Phys. Rev. A **66**, 032701 (2000)
15. D.A. Sharpiro, R. Ciurylo, J.R. Drummond, A.D. May, Phys. Rev. A **65**, 012501 (2001)
16. R. Ciurylo, D.A. Shapiro, J.R. Drummond, A.D. May, Phys. Rev. A **65**, 012502 (2001)
17. D.A. Shapiro, R. Ciurylo, R. Jaworski, A.D. May, Can. J. Phys. **79**, 1209 (2001)
18. J. Keilson, J.E. Storer, Quaterly Appl. Math. **10**, 243 (1952)
19. D.A. Shapiro, J. Phys. B **33**, L43 (2000)
20. M. Abramowitz, I.A. Stegun, *Handbook of Mathematical functions* (Dover Publications Inc., New-York, 1970)
21. A.I. Burshtein, S.I. Temkin, *Spectroscopy of Molecular rotation in gases and liquids* (Cambridge University Press, 1994)
22. W.H. Press, B.P. Flannery, S.A. Tenkolski, W.T. Vetterling, *Numerical recipes* (Cambridge University Press, 1988)
23. F. Chaussard, R. Saint-Loup, H. Berger, P. Joubert, X. Bruet, J. Bonamy, D. Robert, J. Chem. Phys. **113**, 4951 (2000)
24. J. Hussong, R. Lüekerath, W. Stricker, X. Bruet, P. Joubert, J. Bonamy, D. Robert, Appl. Phys. B **73**, 165 (2001)
25. P.M. Sinclair, J.Ph. Berger, X. Michaut, R. Saint-Loup, R. Chaux, H. Berger, J. Bonamy, D. Robert, Phys. Rev. A **54**, 402 (1996)
26. The same numerical method for the resolution of the 3D kinetic equation (cf. Sect. 2) also applies to the KS (monoparametric) velocity memory model [18]. The only significant change is the need to introduce the *generalized* Laguerre Polynomials $\overline{L}_n^{\ell+1/2}(x)$ [20,21] instead of the usual ones $\overline{L}_n^{1/2}(x)$ in order to express the ℓ-components of the velocity-memory function (Eq. (5)) As a direct consequence, the $I_{nn'}$ and $\Gamma_{nn'}$ matrices (Eqs. (15) and (16)) become ℓ-dependent, leading to a slightly more tedious resolution.
27. B. Lance, D. Robert, J. Chem. Phys. **109**, 8283 (1998); J. Chem. Phys. **111**, 789 (1999)
28. J.-M. Hartmann, private communication